

LETTER TO THE EDITOR

Discovery of thiofulminic acid with the QUIJOTE¹ line survey: A study of the isomers of HNCS and HNCO in TMC-1[★]

J. Cernicharo¹, M. Agúndez¹, C. Cabezas¹, B. Tercero^{2,3}, R. Fuentetaja¹, N. Marcelino^{2,3}, and P. de Vicente³

¹ Dept. de Astrofísica Molecular, Instituto de Física Fundamental (IFF-CSIC), C/ Serrano 121, 28006 Madrid, Spain.
e-mail: jose.cernicharo@csic.es

² Observatorio Astronómico Nacional (OAN, IGN), C/ Alfonso XII, 3, 28014, Madrid, Spain.

³ Centro de Desarrollos Tecnológicos, Observatorio de Yebes (IGN), 19141 Yebes, Guadalajara, Spain.

Received: 9 December 2023; accepted: 9 January 2024

ABSTRACT

We present the first detection of HCNS (thiofulminic acid) in space with the QUIJOTE¹ line survey in the direction of TMC-1. We performed a complete study of the isomers of CHNS and CHNO, including NCO and NCS. The derived column densities for HCNS, HNCS, and HSCN are $(9.0\pm 0.5)\times 10^9$, $(3.2\pm 0.1)\times 10^{11}$, and $(8.3\pm 0.4)\times 10^{11}$ cm⁻², respectively. The HNCS/HSCN abundance ratio is 0.38. The abundance ratios HNCO/HNCS, HCNO/HCNS, HOCN/HSCN, and NCO/NCS are 34 ± 4 , 8.3 ± 0.7 , 0.18 ± 0.03 , and 0.78 ± 0.07 , respectively. These ratios cannot be correctly reproduced by our gas-phase chemical models, which suggests that formation paths for these species are missing, and/or that the adopted dissociative recombination rates for their protonated precursors have to be revised. The isotopologues H¹⁵NCO, DNCO, HN¹³CO, DCNO, H³⁴SCN, and DSCN have also been detected with the ultrasensitive QUIJOTE line survey.

Key words. molecular data — line: identification — ISM: molecules — ISM: individual (TMC-1) — astrochemistry

1. Introduction

Among the new species discovered in recent years with the QUIJOTE¹ line survey of TMC-1 (Cernicharo et al. 2021a, 2023a,b, and references therein), it is worth noting that 11 of them are S-bearing species: NCS, HCCS, H₂CCS, H₂CCCS, C₄S, HCSCN, HCSCCH, HC₄S, HC₃S⁺, HCCS⁺, and HSO (Cernicharo et al. 2021b,c,d; Cabezas et al. 2022a; Fuentetaja et al. 2022; Marcelino et al. 2023). The chemical models for S-bearing molecules in interstellar clouds poorly reproduce the observed abundances and the results are strongly dependent on the adopted depletion of sulfur (Vidal et al. 2017). Moreover, many reactions involving S⁺ with neutrals, as well as radicals with S and CS, are missing in the chemical networks and further study is required in order to achieve better agreement between chemical models and observations of sulfur-bearing species (Petrie 1996; Bulut et al. 2021). In addition to these new species, other S-bearing molecules such as CS, SO, NS, NS⁺, HCS⁺, HSC, HCS, CCS, C₃S, C₅S, H₂CS, HSCN, and HNCS are present in TMC-1 (See Table 1 in Cernicharo et al. 2021b). Despite the high depletion of sulphur in molecular clouds, most of these species are the counterpart of the same molecular structure but replacing sulphur with oxygen. Only C₄O, HCCO⁺, and HC₄O have not yet been detected in TMC-1, or indeed in any other source.

HNCS (Frerking et al. 1979) and HSCN (Halfen et al. 2009) are isomers of the CHNS family, and obvious counterparts of the isomers of CHNO. For the latter family, HNCO (Snyder & Buhl 1972), HCNO (Marcelino et al. 2009), and HOCN (Brünken et al. 2009a; Marcelino et al. 2010) have been detected in space in a broad sample of cold and warm molecular clouds.

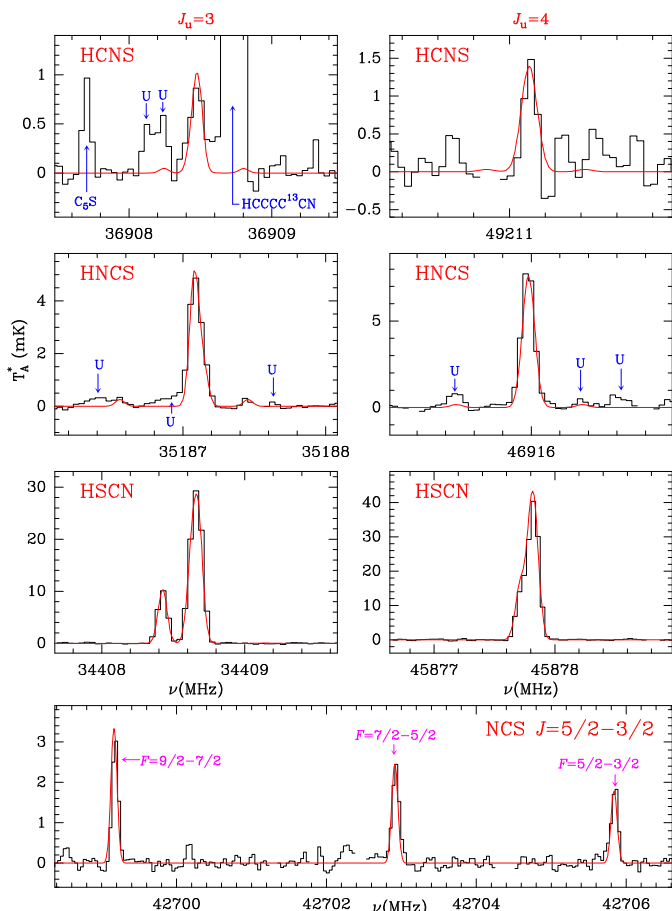
The study of isomers of the same molecule provides clues as to the formation mechanism of these species, as often they are produced from a common precursor. The recent detection of five cyano derivatives of propene, which have energies ranging from 0 to 19.6 kJ/mol (0-2357 K) but similar abundances, indicates that kinetics, and not energetics, is dominating the production of these different isomers (Cernicharo et al. 2022a). The most relevant isomers in space are HCN and HNC, which are assumed to be produced from the dissociative electronic recombination (*DR*) of HCNH⁺. In cold dark clouds, these isomers have an abundance ratio of ~1 in spite of the much higher energy of HNC of 55 kJ/mol (Baulch et al. 2005; Mendes et al. 2012, and references therein). Their chemistry in interstellar clouds was analysed in detail by Loison et al. (2014).

Concerning the CHNS and CHNO isomers, it is assumed that the first are mainly formed from *DR* of H₂NCS⁺ and HNCSH⁺ (Adande et al. 2010; Gronowski & Kolos 2014), and the second from *DR* of H₂NCO⁺ and HNCOH⁺ (Marcelino et al. 2010; Quan et al. 2010). In the present work, we present the first detection of HCNS (thiofulminic acid) in space (TMC-1) and a coherent and precise study of the abundances of the isomers of CHNS and CHNO. The isotopologues H³⁴SCN, DSCN, H¹⁵NCO, HN¹³CO, DNCO, and DCNO are also detected in TMC-1. The derived abundances for the CHNS and CHNO isomers, together with those of NCS and NCO, are compared

[★] Based on observations with the Yebes 40m radio telescope (projects 19A003, 20A014, 20D023, 21A011, 21D005, 22A007, 22B029, and 23A024) and the IRAM 30m radiotelescope. The 40m radiotelescope at Yebes Observatory is operated by the Spanish Geographic Institute (IGN, Ministerio de Transportes y Movilidad Sostenible). IRAM is supported by INSU/CNRS (France), MPG (Germany), and IGN (Spain).

¹ Q-band Ultrasensitive Inspection Journey to the Obscure TMC-1 Environment

with the results of state-of-the-art chemical models for S-bearing species.



Observed $J_u = 3$ and 4 ($K_a = 0$) transitions of the isomers of HCNS. The bottom panel shows the hyperfine components of the $J = 5/2 - 3/2$ transition of NCS in its $^2\Pi_{3/2}$ ground state. The abscissa corresponds to the rest frequency.

The ordinate is the antenna temperature corrected for atmospheric and telescope losses, in mK. Blanked channels correspond to negative features produced when folding the frequency-switched data. The red line shows the computed synthetic spectra for these lines (see Sect. 3). The derived line parameters are given in Table A.1.

2. Observations

The observational data used in this work are part of QUIJOTE (Cernicharo et al. 2021a), a spectral line survey of TMC-1 in the Q-band carried out with the Yebes 40m telescope at the position $\alpha_{J2000} = 4^{\text{h}}41^{\text{m}}41.9^{\text{s}}$ and $\delta_{J2000} = +25^{\circ}41'27.0''$, corresponding to the cyanopolyne peak (CP) in TMC-1. A detailed description of the system is given by Tercero et al. (2021), and details on the QUIJOTE line survey are provided by Cernicharo et al. (2021a, 2023a,b). The data analysis procedure is described by Cernicharo et al. (2022b). The total observing time on source is 1202 hours and the measured sensitivity varies between 0.07 mK at 32 GHz and 0.2 mK at 49.5 GHz.

The main beam efficiency can be given across the Q-Band by $B_{\text{eff}} = 0.797 \exp[-(\nu(\text{GHz})/71.1)^2]$. The forward telescope efficiency is 0.95 and the beam size at half power intensity is $54.4''$ and $36.4''$ at 32.4 and 48.4 GHz, respectively.

In addition to the Q-band data, the isomers of HNCO and HNCS were observed in the millimetre domain with the IRAM 30m telescope and consist of a 3mm line survey that covers the 71.6-116 GHz domain (Cernicharo et al. 2012; Agúndez et al. 2022; Cabezas et al. 2022a; Cernicharo et al. 2023b). The final 3mm line survey has a sensitivity of 2-10 mK. However, at some selected frequencies, the sensitivity is as low as 0.6 mK. The IRAM 30m beam varies between $34''$ and $21''$ at 72 GHz and 117 GHz, respectively, while the beam efficiency takes values of 0.83 and 0.78 at the same frequencies ($B_{\text{eff}} = 0.871 \exp[-(\nu(\text{GHz})/359)^2]$). The forward efficiency at 3mm is 0.95.

The absolute intensity calibration uncertainty is 10%. However, the relative calibration between lines within the QUIJOTE survey is certainly better because all them are observed simultaneously and have the same calibration uncertainties. The data were analysed with the GILDAS package².

3. Results

Line identification in this work was performed using the MADEx code (Cernicharo 2012), and the CDMS and JPL catalogues (Müller et al. 2005; Pickett et al. 1998). The references for the laboratory data used by MADEx in its spectroscopic predictions are described below. The intensity scale used in this study is the antenna temperature (T_A^*). Consequently, the telescope parameters and source properties were used when modelling the emission of the different species in order to produce synthetic spectra in this temperature scale. The permanent dipolar moments of the molecular species studied in this work are given in Table 1. In this work, we assumed a velocity for the source relative to the local standard of rest of 5.83 km s^{-1} (Cernicharo et al. 2020). The source is assumed to be circular with a uniform brightness temperature and a radius of $40''$ (Fossé et al. 2001). The procedure to derive line parameters is described in Appendix A. The observed line intensities were modelled using a local thermodynamical equilibrium hypothesis (LTE), or a large velocity gradient approach (LVG). In the latter case, MADEx uses the formalism described by Goldreich & Kwan (1974).

3.1. The HCNS, HSCN, and HNCS isomers

The HCNS, HNCS, and HSCN isomers were observed with high spectral resolution in the laboratory (Brünken et al. 2009b; McGuire et al. 2016). The frequencies measured in these studies were fitted using the adapted Hamiltonian for each species and the resulting rotational constants were implemented into the MADEx code to predict transition frequencies and to model the observed emission line profiles.

HNCS and HSCN are well-known molecular components of interstellar clouds (Frerking et al. 1979; Halfen et al. 2009; Adande et al. 2010; Vastel et al. 2018). They harbour strong lines in our line survey. However, the isomer HCNS has not been detected yet in space. It is the thio-form of HCNO, an isomer of HNCO and a molecule detected in several interstellar clouds (Marcelino et al. 2009). Thanks to the sensitivity of QUIJOTE, we report in this work the first detection of its two lines in the Q-band ($J = 3 - 2$ and $J = 4 - 3$) in space, namely towards TMC-1. The lines are detected with a signal-to-noise ratio (S/N) of ~ 12 and match the predicted frequencies within 3 kHz (see Fig. 1). The derived line parameters are given in Table A.1. The sensitivity of our line survey at 3mm with the IRAM 30m telescope is not as high as that of QUIJOTE. Nevertheless, the $J = 6 - 5$

² <http://www.iram.fr/IRAMFR/GILDAS>

Table 1. Derived column densities for the isomers of HNCO and HNCS

Species	T_{rot} (K)	μ_a (D)	N^A (cm^{-2})	Notes
HCNS	7.0	3.85	$(9.0\pm 0.5)\times 10^{09}$	a
HNCS	6.0	1.64	$(3.2\pm 0.1)\times 10^{11}$	b
HSCN	5.2	3.33	$(8.3\pm 0.4)\times 10^{11}$	c
HSNC	5.2	3.13	$\leq 4\times 10^{09}$	a
NCS	5.5	2.45	$(9.5\pm 0.2)\times 10^{11}$	d
HNCO	8.0	1.58	$(1.1\pm 0.1)\times 10^{13}$	d
HCNO	5.5	3.10	$(7.8\pm 0.2)\times 10^{10}$	e
HOCN	5.5	3.70	$(1.5\pm 0.2)\times 10^{11}$	f
HONC	5.5	3.13	$\leq 5\times 10^{09}$	g
NCO	8.0	0.64	$(7.4\pm 0.5)\times 10^{11}$	h
H ₂ NCO ⁺	5.5	4.13	$(1.8\pm 0.4)\times 10^{10}$	i
H ³⁴ SCN	5.2	3.33	$(2.1\pm 0.3)\times 10^{10}$	j
DSCN	5.2	3.33	$(2.1\pm 0.3)\times 10^{10}$	j
H ¹⁵ NCO	8.0	1.58	$(3.3\pm 0.3)\times 10^{10}$	j
HN ¹³ CO	8.0	1.58	$(2.1\pm 0.1)\times 10^{11}$	j
DNCO	8.0	1.58	$(2.5\pm 0.2)\times 10^{11}$	j
DCNO	5.5	3.10	$(3.1\pm 0.4)\times 10^{09}$	j

Notes. ^(a) Column densities for the isomers of HCNS, together with the most abundant S-bearing species, were reported by Cernicharo et al. (2021b). The present estimations are $\sim 20\%$ larger due to the recalibration of the QUIJOTE data in 2023 (Cernicharo et al. 2023a). ^(a) μ_a from McGuire et al. (2016). ^(b) μ_a from Szalanski et al. (1978). ^(c) μ_a from Woon & Herbst (2009). ^(d) μ_a from CDMS (Müller et al. 2005). ^(e) μ_a from Takashi et al. (1989). ^(f) μ_a from Brünken et al. (2009a). ^(g) μ_a from Mladenovic et al. (2009). ^(h) μ_a from Saito & Amano (1970). ⁽ⁱ⁾ μ_a from Gupta et al. (2013). ^(j) Assumed identical to that of the main isotopologue.

line of HCNS at 73815.849 MHz is detected at a 3σ level in the data (see Fig. A.1). We also observed this line with the Yebes 40m telescope using the W-band receiver described by Tercero et al. (2021). Near the frequency of the HCNS $J = 6 - 5$ transition, there is a line of CCC¹³CH that is detected with good S/N with both telescopes. It has an intensity of 10 mK and has been used to scale the data of the Yebes 40m and the IRAM 30m telescopes. The two sets of data were merged, weighting them as $1/\sigma^2$. The resulting data allow us to detect the $J = 6 - 5$ line of HCNS at 4σ . The results are shown in Fig. A.1. We conclude that HCNS is convincingly detected in TMC-1. A fit to the laboratory and astronomical frequencies for this species provides the following new molecular constants: $B=6151.44367\pm 0.00027$ MHz, $D=1.712\pm 0.016$ kHz, and $eQq=-0.7227\pm 0.0018$ MHz.

From the observed intensities of these three lines of HCNS, and using a line profile fit method (Cernicharo et al. 2021d), we obtain $T_{rot}=7.0\pm 0.5$ K and $N(\text{HCNS})=(9.0\pm 0.5)\times 10^9 \text{ cm}^{-2}$. The synthetic spectra are shown in Fig. 1 and A.1, and are in excellent agreement with the observations. No collisional rates are available for HCNS, but with the aim to estimate the excitation conditions that could be expected for this molecule in the LVG approximation, we adopted the collisional rates of OCS with H₂ calculated by Green & Chapman (1978). OCS has a rotational constant similar to that of HCNS, and therefore we consider that these rates provide a better approximation to those of HCNS than the rates of HCNO (Naindoubi et al. 2015), which has a rotational constant twice that of HCNS. For the typical volume densities of TMC-1 of $1\times 10^4 \text{ cm}^{-3}$ (Agundez et al. 2023, Fuentetaja et al., in prep.), we obtain that the excitation temperatures of the observed lines could vary between 8.2 K for the $J = 3 - 2$ line

down to 6.2 K for the $J = 6 - 5$ transition, in good agreement with the derived averaged rotational temperature of 7 K.

The $J_u = 3, 4$ with $K_a = 0$ transitions of HNCS and HSCN appear in our QUIJOTE data as features exhibiting all their hyperfine components with a very high S/N. These transitions are shown in Fig. 1. The corresponding $K_a = 1$ lines of HNCS have upper energy levels of 66 ($J_u = 3$) and 68 K ($J_u = 4$) and are not detected in our data. However, the corresponding energies for HSCN are only at 16.9 and 19.2 K, respectively. We detected these latter; they are shown in Fig. A.2. Moreover, the $J_u = 7, 8$ transitions with $K_a=0$ of both isomers were detected with the IRAM 30m telescope (see Fig. A.2). The derived line parameters for all these lines are given in Table A.1. No collisional rates are available for either of the two isomers. We used all observed lines using the line profile fitting procedure (Cernicharo et al. 2021d) to derive their rotational temperature and column densities. For HNCS, we obtain $T_{rot}=6.0\pm 0.5$ K and $N(\text{HNCS})=(3.2\pm 0.1)\times 10^{11} \text{ cm}^{-2}$. For HSCN, we derived $T_{rot}=5.2\pm 0.3$ K and $N(\text{HSCN}, K_a=0) = (6.9\pm 0.2)\times 10^{11} \text{ cm}^{-2}$, and $N(\text{HSCN}, K_a=1) = (1.4\pm 0.3)\times 10^{11} \text{ cm}^{-2}$. The interladder temperature between $K_a=0$ and 1 lines could be thermalised by collisions at the kinetic temperature of the cloud. For an energy separation between these ladders of 14.5 K, we derive a kinetic temperature for TMC-1 of 9.1 ± 1.5 K, which is in excellent agreement with the result obtained by Agundez et al. (2023).

The isomer HSNC has been characterised in the laboratory (McGuire et al. 2016) and we searched for its lines in our survey. However, we only obtained an upper limit of $4\times 10^9 \text{ cm}^{-2}$ for its column density. Of particular interest for the chemistry of the CHNS isomers, it is worth deriving the column density of NCS as it could participate in their formation. NCS was discovered in TMC-1 with previous QUIJOTE line data (Cernicharo et al. 2021b). The new data are shown in Fig. 1. Adopting a rotational temperature of 5.5 K, the derived column density is $(9.5\pm 0.2)\times 10^{11} \text{ cm}^{-2}$. The NCS to HNCS abundance ratio is 3.0 ± 0.16 .

Among the isomers of the CHNS family, the most abundant is HSCN. Its lines are strong enough to allow a search for its isotopologues. We observed two rotational transitions exhibiting hyperfine structure for H³⁴SCN and DSCN (see Fig. A.3). Adopting the same rotational temperature as for the main isotopologue, we derive the column densities given in Table 1. The ³²S/³⁴S abundance ratio is 33 ± 5 , which agrees with previous determinations using other molecular species (see e.g. Cernicharo et al. 2021b and Fuentetaja et al. in prep., and references therein). The H/D abundance ratio is also 33 ± 5 and represents a considerable single deuterium enhancement in HSCN, in line with that observed in other molecules in TMC-1 (Cabezas et al. 2021, 2022b, and references therein).

3.2. The HNCO, HCNO, and HOCN isomers

HNCO was one of the first molecules detected in the early years of millimetre radio astronomy by Snyder & Buhl (1972). Its isomer HCNO (fulminic acid) was detected by Marcelino et al. (2009) towards B1, L1544, and L183, but not in TMC-1. Another isomer, HOCN, was detected towards SgrB2, B1-b, L1544, L1527, L183, and IRAS16293-2422 (Brünken et al. 2009a, 2010; Marcelino et al. 2010). Therefore, these isomers have been detected in space in a broad sample of cold and warm molecular clouds. The level energies, transition frequencies, and intensities for HNCO and its isotopologues, as well as for HOCN, are from the JPL and CDMS catalogues, respectively. HCNO is a quasi-linear molecule and its rotational fre-

quencies were obtained from a fit to available laboratory data (Winnewisser & Winnewisser 1971). The three isomers and the isotopologues ^{15}N , ^{13}C , and D of HNCO have been detected with QUIJOTE in TMC-1. The data are shown in Fig. A.4 and the derived line parameters are given in Table A.2. We note that for HN^{13}CO and DNCO, our measured frequencies have a significant lower uncertainty than those in the entries of the JPL catalogue.

The HNCO lines are the strongest among those of all its isomers. We also detected the $4_{04} - 3_{03}$ and $5_{05} - 4_{04}$ lines at 3mm with the IRAM 30m radio telescope. These lines are shown in Fig. A.5. Collisional rates for HNCO with He ($T_K \geq 30$ K; Green 1986) and H_2 ($T_K \geq 7$ K; Sahnoun et al. 2018) are available. For a volume density of $1\text{--}2 \times 10^4$, our LVG calculations using the $p\text{--H}_2$ collisional rates provide excitation temperatures for the $2_{0,2} - 1_{0,1}$ line of HNCO of 8–9 K, decreasing to ~ 5 K for the $5_{05} - 4_{04}$ transition. We therefore adopted a rotational temperature of 8 K for HNCO and its isotopologues in the Q-band, and of 4.8 K in the 3mm domain. The derived column densities are given in Table 1 and the computed synthetic spectra are shown in red in Figures A.4 and A.5. The HNCO/ HN^{13}CO , HNCO/DNCO, and HNCO/ H^{15}NCO abundance ratios are 52 ± 8 , 44 ± 8 , and 333 ± 60 .

The isomers HCNO and HOCN have dipolar moments of 3.1 and 3.7 D, respectively (see Table 1). For HCNO we used the LVG approximation using the collisional rates of HCNO with He calculated by Naindoubia et al. (2015). For a density of $1\text{--}2 \times 10^4 \text{ cm}^{-3}$, we obtain rotational temperatures in the range of 4.9–5.5 K. HCNO is detected for the first time in TMC-1. We also observed its $J = 4 - 3$ transition at 3mm (see Fig. A.2). The estimated column density for this isomer of HNCO is $(7.8 \pm 0.2) \times 10^{10} \text{ cm}^{-2}$. We also observed the $J = 2 - 1$ of DCNO in the Q-band (see Fig. A.5). The derived HCNO/DCNO abundance ratio is 25 ± 4 . For HOCN, we observed the $2_{0,2} - 1_{0,1}$ with QUIJOTE and its $4_{04} - 3_{03}$ and $5_{05} - 4_{04}$ lines at 3mm (see Fig. A.5). All the observed lines are well reproduced by the models with a rotational temperature similar to that of HCNO ($T_{rot} = 5.5$ K) as shown by the computed synthetic spectra shown in Figures A.4 and A.5. The derived column densities for HCNO and HOCN are given in Table 1. The fundamental transition of HOCN at 20.9 GHz was tentatively observed in TMC-1 by Brünken et al. (2009b).

We detected the four strongest hyperfine components of the $J = 7/2 - 5/2$ transition of NCO in its $^2\Pi_{3/2}$ ground state at 3mm. This species was recently detected towards L483 by Marcelino et al. (2018) with an NCO/HNCO abundance ratio of ~ 0.2 . Due to the modest dipole moment of this species ($\mu = 0.64$ D; Saito & Amano 1970), we modelled the TMC-1 data adopting $T_{rot}(\text{NCO}) = 8$ K. The derived column density is $(7.4 \pm 0.5) \times 10^{11} \text{ cm}^{-2}$ and the NCO/HNCO abundance ratio is 0.067, which is three times lower than towards L483. However, in TMC-1 the NCS/HNCS ratio is 45 times larger than the NCO/HNCO one. We also searched for the isomer HONC (Mladenovic et al. 2009), but only obtained upper limits (see Table 1). Finally, three lines of H_2NCO^+ were observed in the Q-band. These are shown in Fig. A.6 and their line parameters are given in Table A.2. Adopting a rotational temperature of 5.5 K and a o/p abundance ratio of 3:1, the derived total column density for this species is $(1.8 \pm 0.4) \times 10^{10} \text{ cm}^{-2}$.

4. Discussion

The most energetically stable isomer of the CHNS family is HNCS, followed by HSCN, HCNS, and HSNC at 3171, 17317, and 18120 K above, respectively (Wierzejewska & Moc 2003;

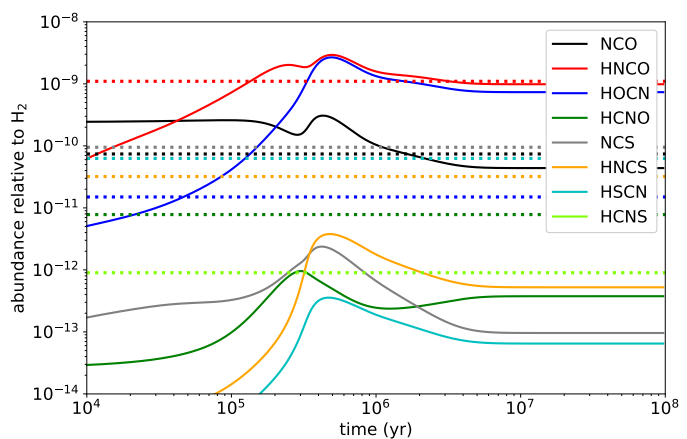
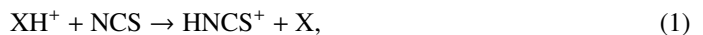


Fig. 1. Abundances calculated with the chemical model for molecules of the families of HNCO and HNCS. The peak calculated abundance of HCNS is around 10^{-15} relative to H_2 and therefore lies outside the abundance range shown. Horizontal dashed lines correspond to the abundances observed in TMC-1.

McGuire et al. 2016). The energy ordering in the oxygen family is similar, with HNCO being the most stable isomer, and HOCN, HCNO, and HONC lying at 12330, 34480, and 42235 K above, respectively (Schuurman et al. 2003). In spite of the similarities in the energetics, the CHNO and CHNS families show a very different behaviour in TMC-1. While HNCO is far more abundant than HOCN, the abundance of HNCS is only half of that of HSCN (see Table 2).

The chemistry of HNCS and its isomers has been discussed by Adande et al. (2010), Gronowski & Kolos (2014), and Vidal et al. (2017). Here, we revisit the subject by running a gas-phase chemical model of a cold dense cloud (see details in Cernicharo et al. 2021b and Fuentetaja et al. 2022). The chemical scheme of synthesis of HNCS and HSCN can be summarized as



where the scheme begins with the protonation of NCS by abundant proton donors XH^+ , such as HCO^+ , H_3O^+ , and H_3^+ . This scheme, replacing sulfur by oxygen, is the same one that describes the formation of the oxygen analogues HNCO and HOCN (Marcelino et al. 2010; Quan et al. 2010; Lattanzi et al. 2012). The chemical scheme starts with the radicals NCO and NCS, which are mostly formed through neutral–neutral reactions. According to the chemical model, the main reactions forming NCO are $\text{N} + \text{HCO}$ and $\text{CN} + \text{O}_2$, while NCS is mainly formed through the analogous reactions $\text{N} + \text{HCS}$ and $\text{CN} + \text{SO}$.

The abundances calculated with the chemical model are shown in Fig. 1. We focus on times around a few 10^5 yr, when most molecules reach their peak abundances. The abundances calculated for NCO and HNCO are in line with the observed values. In the case of HOCN, the calculated abundance is close

Table 2. Derived abundance ratios for the isomers of HNCO and HNCS in TMC-1

S-species	N(X)/N(HNCS)	O-species	N(X)/N(HNCO)	N(S)/N(O)
HCNS	0.028±0.002	HCNO	0.0071±0.0008	0.12±0.01
HNCS	1.0	HNCO	1.0	0.029±0.004
HSCN	2.60±0.016	HOCN	0.014±0.003	5.52±0.91
HSNC	≤0.013	HONC	≤0.0005	
NCS	3.00±0.16	NCO	0.067±0.011	1.28±0.11
NS ^a	5.3±0.7	NO ^b	25±6	0.007±0.002
		H ₂ NCO ⁺	0.0016±0.0005	

Notes. ^(a) Column density of $(1.7±0.2)×10^{12}$ cm⁻² (Cernicharo et al. 2018). ^(b) Column density of $(2.7±0.5)×10^{14}$ cm⁻² (Gerin et al. 1993).

to that of HNCO, while observations indicate that HOCN is much less abundant than HNCO. It is likely that the dissociative recombination of HNCOH⁺ favours HNCO over HOCN (the model assumes equal branching ratios) or that the reaction between HNCOH⁺ and H₂ favours H₂NCO⁺ over HNCOH⁺ (equal yields are assumed at present). Investigation into these two reactions would allow us to understand the high observed HNCO/HOCN ratio. Grain surface chemistry may also be responsible for this. Indeed, the gas-grain model of Quan et al. (2010) predicted HNCO to be somewhat more abundant than HCNO. The detection of the precursors H₂NCO⁺ and HNCOH⁺ would also be very useful to shed light on this. While the H₂NCO⁺ cation has been detected in interstellar clouds (Gupta et al. 2013; Marcelino et al. 2018), its isomer HNCOH⁺ is still awaiting detection in space (laboratory frequencies are available from Mladenovic et al. 2009). Only the H₂NCO⁺ cation is detected in our TMC-1 data.

In the case of the sulfur analogues NCS, HNCS, and HSCN, the model severely underestimates their abundances. It is likely that the model lacks efficient routes to NCS, hampering the subsequent formation of HNCS and HSCN. A similar situation was encountered in previous chemical models, with abundances relative to H₂ < 10⁻¹² for HNCS and HSCN (Adande et al. 2010; Gronowski & Kolos 2014; Vidal et al. 2017). Apart from the general problem of abundance underestimation, the fact that HSCN is observed to be more abundant than HNCS, in contrast to the oxygen case, indicates that the branching ratios of reactions (2) and (4) must be markedly different to those of the analogous oxygen reactions. Identification of the precursor cations H₂NCS⁺ and HNCSH⁺ would also help to constrain the chemistry of HNCS and HSCN, although their rotational spectrum has not yet been characterised in the laboratory.

The third observed species of the family of HNCO isomers, namely HCNO, has a different skeleton to the other two isomers and is therefore formed in a different way. According to the chemical model, the neutral-neutral reaction CH₂ + NO (Marcelino et al. 2009) is the main source of HCNO. The analogous molecule with sulfur, HCNS (the one reported here), is severely underestimated by the chemical model. The analogous reaction CH₂ + NS cannot account for HCNS because in TMC-1, NS is 160 times less abundant than NO, while HCNS is just 9 times less abundant than HCNO (see Table 2). Among the potential missing routes to HCNS, we could consider the neutral-neutral reactions HCN + SH, CN + H₂S, N + H₂CS, NH + HCS, and NH₂ + CS. To our knowledge, these reactions have not been studied either theoretically or experimentally, and therefore we do not know whether or not they are fast at low temperatures and produce HCNS as a product. Among these reactions, the most efficient by far is N + H₂CS, which would provide an HCNS abundance of the order of the observed one assuming that it has

a rate coefficient of the order of $1×10^{-10}$ cm³ s⁻¹ at low temperature.

We conclude that further experimental and theoretical work is needed to understand the chemistry of the HNCS and HNCO isomers. In particular, the enhancement of the abundance of HSCN relative to HNCS and HOCN, as well as the behaviour of the NCS/HNCS and NCO/HNCO abundance ratios, are not well reproduced by the present chemical models.

Acknowledgements. We thank Ministerio de Ciencia e Innovación of Spain (MICIU) for funding support through projects PID2019-106110GB-I00, and PID2019-106235GB-I00. We also thank ERC for funding through grant ERC-2013-Syg-610256-NANOCOSMOS.

References

- Adande, G.R., Halfen, D.T., Ziurys, L.M. et al. 2010, *ApJ*, 725, 561
 Agúndez, M., Cabezas, C., Marcelino, N. et al. 2022, *A&A*, 659, L9
 Agúndez, M., Marcelino, N., Tercero, B. et al. 2023, *A&A*, 677, A106
 Baulch D.L., Bowman C.T., Cobos C.J., et al., 2005, *J. Phys. Chem. Ref. Data*, 34, 757
 Brünken, S., Gottlieb, C.A., McCarthy, M.C. & Thaddeus, P. 2009a, *ApJ*, 697, 880
 Brünken, S., Yu, Z., Gottlieb, C.A., et al. 2009b, *ApJ*, 706, 1588
 Brünken, S., Belloche, A., Martín, S. et al. 2010, *A&A*, 516, A109
 Bulut, N., Roncero, O., Aguado, A., et al. 2021, *A&A*, 646, A5
 Cabezas, C., Roueff, E., Tercero, B. et al. 2021, *A&A*, 650, L15
 Cabezas, C., Agúndez, M., Marcelino, N., et al. 2022a, *A&A*, 657, L4
 Cabezas, C., Agúndez, M., Marcelino, N., et al. 2022b, *A&A*, 657, L5
 Cernicharo, J., Marcelino, N., Roueff, E., et al. 2012, *ApJ*, 759, L43
 Cernicharo, J., 2012, in *ECLA 2011: Proc. of the European Conference on Laboratory Astrophysics*, EAS Publications Series, 2012, Ed.: C. Stehl, C. Joblin, & L. d'Hendecourt (Cambridge: Cambridge Univ. Press), 251; https://nanocosmos.iff.csic.es/?page_id=1619
 Cernicharo, J., Lefloch, B., Agúndez, M. et al. 2018, *ApJ*, 853, L22
 Cernicharo, J., Marcelino, N., Agúndez, M. et al. 2020, *A&A*, 642, L8
 Cernicharo, J., Agúndez, M., Kaiser, R., et al. 2021a, *A&A*, 652, L9
 Cernicharo, J., Cabezas, C., Agúndez, M. et al. 2021b, *A&A*, 648, L3
 Cernicharo, J., Cabezas, Endo, Y. et al. 2021c, *A&A*, 650, L14
 Cernicharo, J., Cabezas, Endo, Y. et al. 2021d, *A&A*, 646, L3
 Cernicharo, J., Fuentetaja, R., Cabezas, C. et al. 2022a, *A&A*, 663, L5
 Cernicharo, J., Fuentetaja, R., Agúndez, M. et al. 2022b, *A&A*, 663, L9
 Cernicharo, J., Pardo, J.R., Cabezas, C. et al. 2023a, *A&A*, 670, L19
 Cernicharo, J., Agúndez, M., Fuentetaja, R. et al. 2023b, *A&A*, in press
 Fossé, D., Cernicharo, J., Gerin, M., Cox, P. 2001, *ApJ*, 552, 168
 Frerking, M.A., Linke, R.A. & Thaddeus, P. 1979, *ApJ*, 234, L143
 Fuentetaja, R., Agúndez, M., Cabezas, C. et al. 2022, *A&A*, 667, L4
 Gerin, M., Viala, Y. & Casoli, F. 1993, *A&A*, 268, 212
 Goldreich, P. & Kwan, J. 1974, *ApJ*, 189, 441
 Green, S. & Chapman, S. 1978, *ApJS*, 37, 169
 Green, S. 1986, NASA Technical Memorandum, NASA TM 87791
 Gronowski, M. & Kolos R. 2014, *ApJ*, 792, 89
 Gupta, H., Gottlieb, C.A., Lattanzi, V. et al. 2013, *ApJ*, 778, L1
 Halfen, D.T., Ziurys, L.M., Brünken, S. et al. 2009, *ApJ*, 702, L124
 Lattanzi, V., Thorwirth, S., Gottlieb, C. A., & McCarthy, M. C. 2012, *J. Phys. Chem. Lett.*, 3, 3420
 Loison, J.-C., Wakelam, V. & Hickson, K.M. 2014, *MNRAS*, 443, 398
 McGuire, B.A., Martin-Drumel, M.-A., Thorwirth, S. et al. 2016, *PCCP*, 18, 22693
 Marcelino, N., Cernicharo, J., Tercero, B. & Roueff, E. 2009, *ApJ*, 690, L27

- Marcelino, N., Brünken, S., Cernicharo, J. et al. 2010, A&A, 516, A105
- Marcelino, Agúndez, M. Cernicharo, J. et al. 2018, A&A, 612, L10
- Marcelino, Puzzarini, C., Agúndez, M. et al. 2023, A&A, 674, L13
- Mendes, M., Buhr, H. & Berg, M. 2012, ApJ, 746, L8
- Mladenovic, M., Lewerenz, M., McCarthy, M.C. & Thaddeus, P. 2009, J. Chem. Phys. 131, 174308
- Müller, H. S. P., Schlöder, F., Stutzki, J., Winnewisser, G. 2005, J. Mol. Struct., 742, 215
- Naindoubi, A., Nkem, C., Ajili, Y. et al. 2015, Chem. Phys. Lett., 636, 67
- Petrie, S. 1996, MNRAS, 281, 666
- Pickett, H.M., Poynter, R. L., Cohen, E. A., et al. 1998, J. Quant. Spectrosc. Radiat. Transfer, 60, 883
- Quan, D., Herbst, E., Osamura, Y., et al. 2010, ApJ, 725, 2101
- Sahnoun, E., Wiesenfeld, L., Hammami, K. & Jadane, N. 2018, J. Phys. Chem. A, 122, 3004
- Saito, S. & Amano, T. 1970, J. Mol. Spectrosc., 34, 383
- Schuurman, M.S., Muir, S.R., Allen, W.D. & Schaefer III, H.F. 2003, J. Chem. Phys., 120, 11586
- Snyder, L.E. & Buhl, D. 1972, ApJ, 177, 619
- Szalanski, L.B., Gerry, M.C.L., Winnewisser, G. et al. 1978, Can. J. Phys., 56, 1297
- Takashi, R., Tanaka, K. & Tanaka, T. 1989, J. Mol. Spectrosc., 138, 450
- Tercero, F., López-Pérez, J. A., Gallego, et al. 2021, A&A, 645, A37
- Vastel, C., Quénard, D., Le Gal, R. et al. 2018, MNRAS, 4778, 5514
- Vidal, T.H.G., Loison, J.-C., Jaziri, A. Y. et al. 2017, MNRAS, 469, 435
- Wierzejewska, M. & Moc, J. 2003, J. Chem. Phys. A, 107, 11209
- Winnewisser, M. & Winnewisser, B.P. 1971, Z. Naturforsch, 26a, 128
- Woon, D.E. & Herbst, E. 2009, ApJS, 185, 273

Appendix A: Line parameters

Line parameters for all observed transitions with the Yebes 40m and IRAM 30m radio telescopes were derived by fitting a Gaussian line profile to them using the GILDAS package. A velocity range of $\pm 20 \text{ km s}^{-1}$ around each feature was considered for the fit after a polynomial baseline was removed. Negative features produced in the folding of the frequency switching data were blanked before baseline removal.

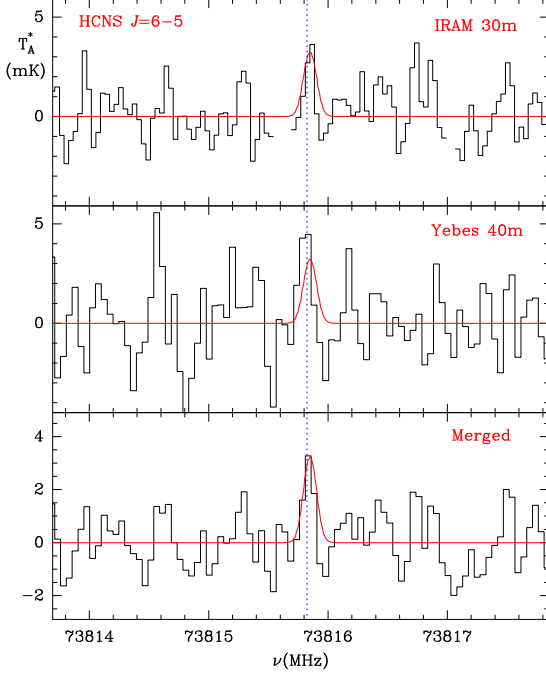


Fig. A.1. Observed $J = 6 - 5$ line of HCNS with the IRAM 30m (top panel) and Yebes 40m (middle panel) radio telescopes. The data of the Yebes telescope have been scaled to those of IRAM using the line $N = 8 - 7$ $J = 15/2 - 13/2$ of CCC^{13}CH at 73819.18 MHz that appears in both sets of data with a S/N of ~ 10 in the IRAM data and of ~ 5 in the Yebes data. The merged spectrum was obtained by averaging both sets of data weighted as $1/\sigma^2$ and has a sensitivity of 1 mK. The derived line parameters for this transition of HCNS are given in Table A.1. The red line corresponds to the computed synthetic spectra (see Sect. 3). The vertical blue line corresponds to the measured frequency for a v_{LSR} of 5.83 km s^{-1} .

The derived line parameters for all observed lines of the CHNS and CHNO families are given in Tables A.1 and A.2, respectively. The differences between the measured frequencies and the predicted ones are always of a few kHz. However, for some isotopologues, several hyperfine components are blended in the laboratory data (measurements with uncertainties $\geq 30 \text{ kHz}$), while in our observations the lines are well resolved and have an uncertainty of 10 kHz.

The lines of HCNS, HNCS, HSCN, and NCS are shown in Figures 1 and A.2. The observations of the $J = 6 - 5$ line of HCNS with the IRAM 30m and the Yebes 40m radio telescopes, together with the resulting merged data, are shown in Fig. A.1. Finally, the lines of the isotopologues H^{34}SCN and DSCN are shown in Fig. A.3. The lines of HNCO, HCNO, HOCN, and NCO are shown in Fig. A.4 and those of H_2NCO^+ in Fig. A.6

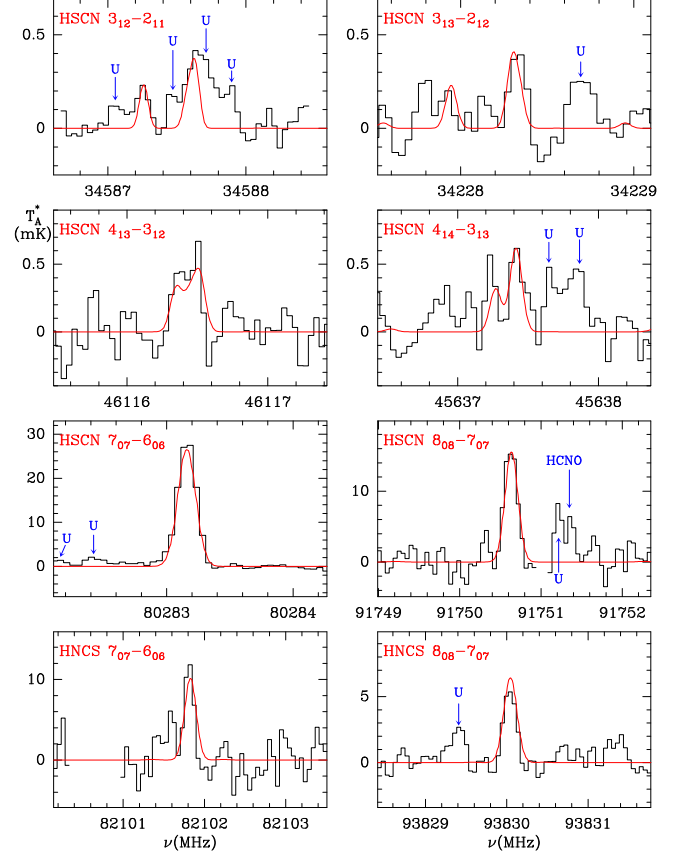


Fig. A.2. Observed lines of HSCN and HNCS. The two upper rows show the observed lines of HSCN with $K_a=1$. The two lower rows show the $7_{07} - 6_{06}$ and $8_{08} - 7_{07}$ lines of HSCN (third row) and HNCS (fourth row) observed at 3mm with the IRAM 30m radio telescope. The red line shows the computed synthetic spectra for these lines (see Sect. 3). The derived line parameters are given in Table A.1.

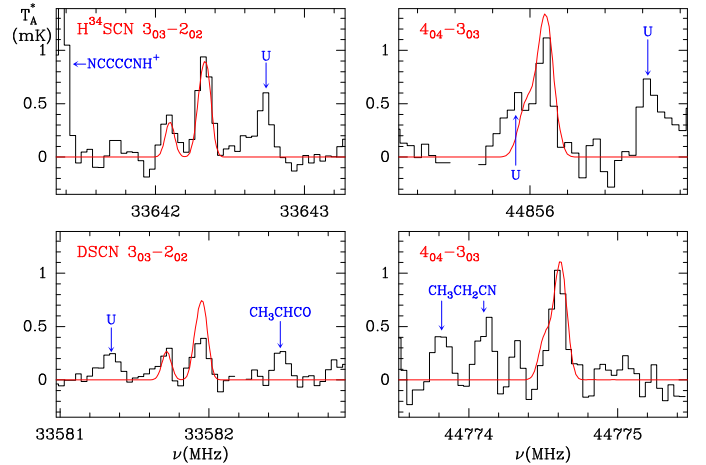


Fig. A.3. Observed $3_{03} - 2_{02}$ and $4_{04} - 3_{03}$ transitions of the isotopologues H^{34}SCN (top panels) and DSCN (bottom panels) of HSCN. The red line shows the computed synthetic spectra for these lines (see Sect. 3). The derived line parameters are given in Table A.1.

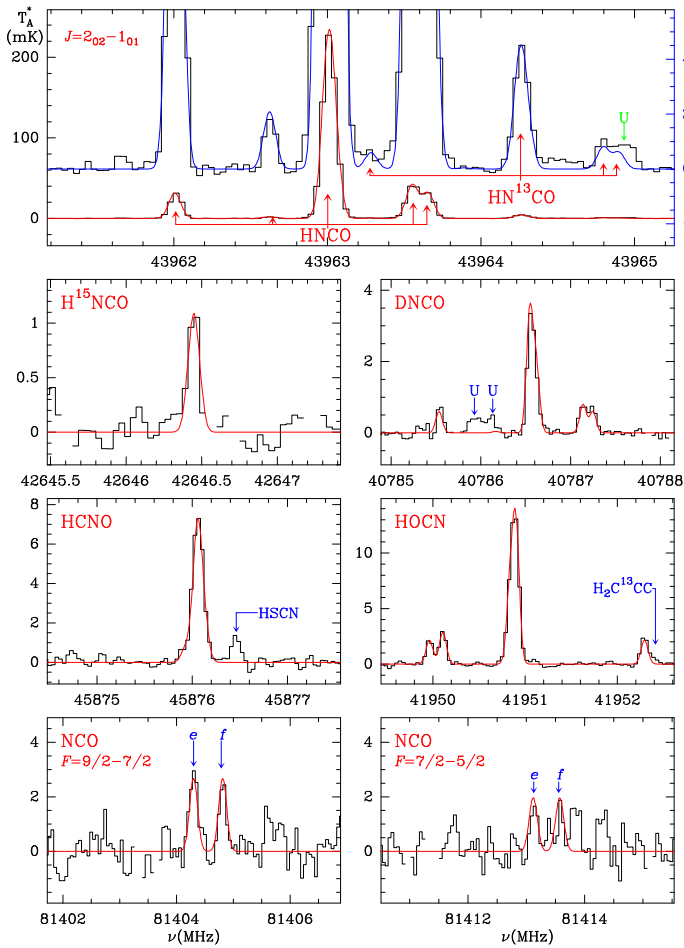


Fig. A.4. Same as Fig. 1 but for the $J = 2_{02} - 1_{01}$ transition of HNCO (isocyanic acid) and its isotopologues HN^{13}CO , H^{15}NCO , and DCNO (upper and second row panels). The upper panel also shows a zoom to the data to exhibit the hyperfine lines of HN^{13}CO . The scale of the zoom is indicated in blue on the right-Y axis. The third row shows the $J = 2 - 1$ line of HCNO (the $J = 4 - 3$ is shown in Fig. A.2) and the $J = 2_{02} - 1_{01}$ line of HOCN (cyanic acid). Finally, the bottom panels show two hyperfine components of the $J=7/2-5/2$ line of NCO in its $^2\Pi_{3/2}$ ground state. The lambda-type doubling components, e and f , are indicated. The derived line parameters are given in Table A.2. The hyperfine structure was considered in the modelling of the lines (shown by the red lines).

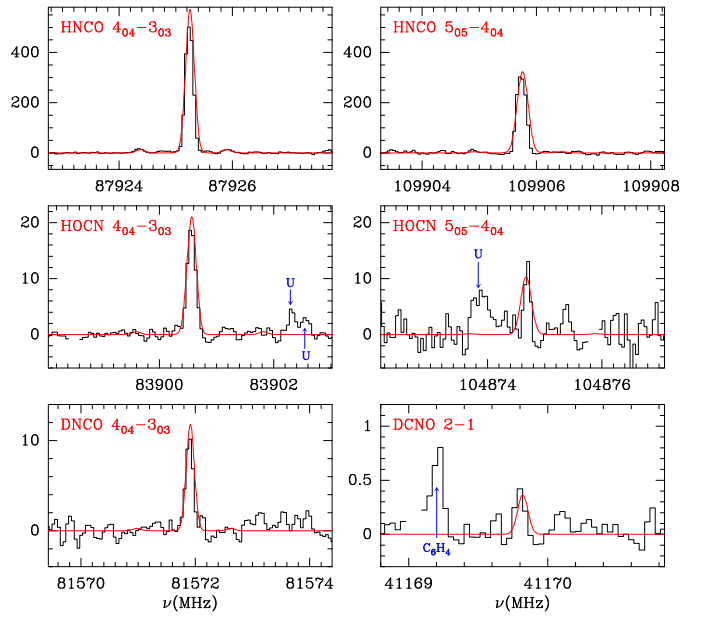


Fig. A.5. Observed lines of HNCO and HOCN at 3mm with the IRAM 30m radio telescope. The red line shows the synthetic spectra computed with the models described in Sect. 3. The column densities are the same as those derived from the lines observed in the Q-band. The bottom panels show the DNCO $4_{04} - 3_{03}$ and DCNO $J = 2 - 1$ lines. The derived line parameters are given in Table A.2.

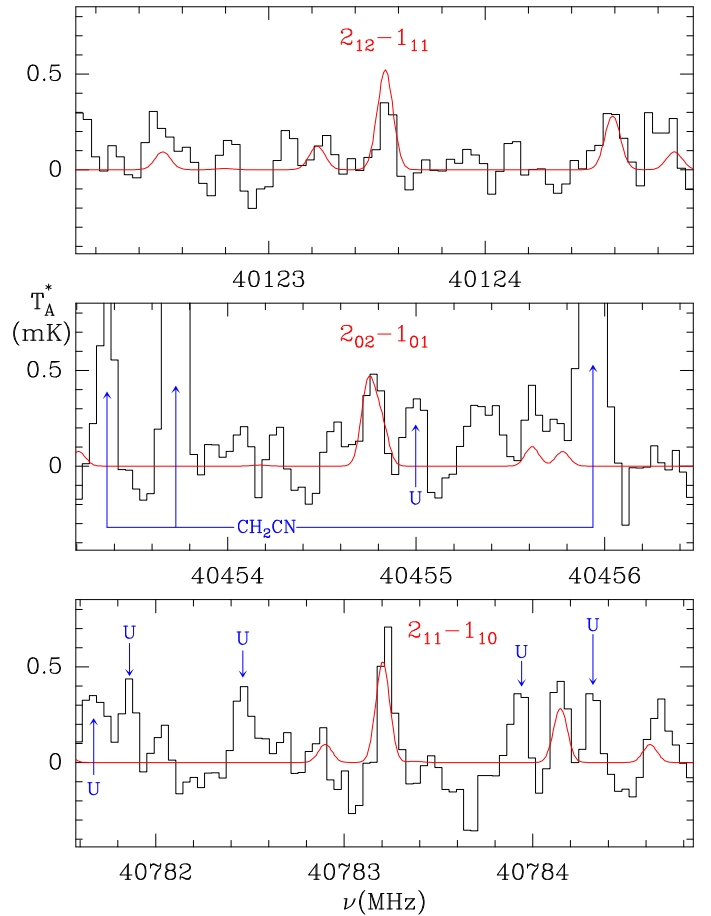


Fig. A.6. Observed $J_u = 2$ lines of H_2NCO^+ towards TMC-1. The red line shows the computed synthetic spectra for these lines (see Sect. 3). The derived line parameters are given in Table A.2.

Table A.1. Observed line parameters for the isomers and isotopologues of HNCS

Species	$J_u - J_l$	$F_u - F_l^a$	ν_{rest}^b (MHz)	$\int T_A^* dv^c$ (mK km s ⁻¹)	v_{LSR} (km s ⁻¹)	Δv^d (km s ⁻¹)	T_A^{*e} (mK)	Notes
HCNS	3-2		36908.475±0.010	0.95±0.06	5.83	1.04±0.09	0.85±0.07	
	4-3		49211.115±0.010	0.77±0.11	5.83	0.47±0.08	1.56±0.14	
	6-5		73815.835±0.020	1.34±0.39	5.83	0.38±0.10	3.40±0.90	
HNCS	3 ₀₃ - 2 ₀₂	2-2	35186.557±0.010	0.19±0.06	5.83	0.63±0.10	0.29±0.07	
		Main	35187.089±0.010	5.05±0.06	5.83	0.99±0.09	4.82±0.07	
		3-3	35187.445±0.010	0.16±0.04	5.83	0.46±0.11	0.33±0.07	
	4 ₀₄ - 3 ₀₃	3-3	46915.466±0.010	0.67±0.10	5.83	0.72±0.13	0.87±0.14	A
		Main	46915.976±0.010	5.98±0.11	5.83	0.68±0.05	8.19±0.14	
		4-4	46916.349±0.010	0.27±0.10	5.83	0.51±0.23	0.50±0.14	A
	7 ₀₇ - 6 ₀₆	Main	82101.810±0.010	6.04±0.09	5.83	0.45±0.07	12.68±2.10	
	8 ₀₈ - 7 ₀₇	Main	93830.036±0.010	3.29±0.16	5.83	0.53±0.04	5.83±0.60	
HSCN	3 ₁₃ - 2 ₁₂	3-2	34227.919±0.020	0.14±0.06	5.83	0.62±0.12	0.21±0.09	
	3 ₁₃ - 2 ₁₂	Main	34228.329±0.010	0.39±0.06	5.83	0.84±0.14	0.44±0.09	
	3 ₀₃ - 2 ₀₂	3-3	34407.322±0.010	1.62±0.09	5.83	0.77±0.04	1.98±0.11	
	3 ₀₃ - 2 ₀₂	2-1	34408.425±0.010	7.74±0.08	5.83	0.72±0.01	10.26±0.11	
	3 ₀₃ - 2 ₀₂	Main	34408.660±0.010	28.58±0.09	5.83	0.90±0.01	29.82±0.11	
	3 ₀₃ - 2 ₀₂	2-2	34410.448±0.010	1.38±0.09	5.83	0.67±0.04	1.93±0.11	
	3 ₁₂ - 2 ₁₁	3-2	34587.252±0.010	0.27±0.05	5.83	1.02±0.21	0.24±0.06	
	3 ₁₂ - 2 ₁₁	Main	34587.606±0.010	0.35±0.05	5.83	1.53±0.32	0.21±0.06	B
	4 ₁₄ - 3 ₁₃	4-3	45637.236±0.010	0.28±0.07	5.83	0.45±0.14	0.57±0.14	
	4 ₁₄ - 3 ₁₃	Main	45637.423±0.010	0.51±0.09	5.83	0.81±0.18	0.59±0.14	
	4 ₀₄ - 3 ₀₃	4-4	45876.458±0.010	0.80±0.07	5.83	0.61±0.05	1.24±0.14	
	4 ₀₄ - 3 ₀₃	3-2	45877.725±0.010	10.52±0.34	5.83	0.68±0.02	14.57±0.14	
	4 ₀₄ - 3 ₀₃	Main	45877.828±0.010	27.29±0.34	5.83	0.65±0.01	39.75±0.14	
	4 ₀₄ - 3 ₀₃	3-3	45878.621±0.010	0.39±0.08	5.83	0.88±0.08	0.41±0.14	
	4 ₁₃ - 3 ₁₂	4-3	46116.344±0.020	0.18±0.04	5.83	0.60±0.00	0.30±0.13	C
	4 ₁₃ - 3 ₁₂	3-2	46116.396±0.020	0.28±0.07	5.83	0.60±0.00	0.31±0.13	C
	4 ₁₃ - 3 ₁₂	5-4	46116.492±0.020	0.36±0.07	5.83	0.60±0.00	0.60±0.13	C
	7 ₀₇ - 6 ₀₆	Main	80283.160±0.010	19.98±0.44	5.83	0.61±0.02	28.89±0.64	
8 ₀₈ - 7 ₀₇	Main	80283.160±0.010	10.54±0.77	5.83	0.60±0.05	16.63±1.66		
DSCN	3 ₁₃ - 2 ₁₂	Main	33258.268±0.010	0.24±0.07	5.83	0.72±0.21	0.32±0.09	
	3 ₀₃ - 2 ₀₂	Main	33581.957±0.010	0.33±0.04	5.83	0.87±0.11	0.35±0.06	D
	3 ₁₂ - 2 ₁₁	Main	33905.771±0.003				≤0.3	
	4 ₁₄ - 3 ₁₃	Main	44343.744±0.010	0.36±0.12	5.83	0.66±0.26	0.52±0.10	
	4 ₀₄ - 3 ₀₃	Main	44774.598±0.010	0.84±0.13	5.83	0.78±0.14	1.01±0.13	
	4 ₁₃ - 3 ₁₂	Main	45207.143±0.010	0.29±0.07	5.83	0.46±0.14	0.60±0.11	
H ³⁴ SCN	3 ₀₃ - 2 ₀₂	2-1	33642.089±0.020	0.39±0.07	5.83	0.91±0.17	0.40±0.07	
	3 ₀₃ - 2 ₀₂	Main	33642.328±0.010	0.98±0.07	5.83	0.96±0.09	0.96±0.07	
	4 ₀₄ - 3 ₀₃	Main	44856.085±0.020	0.64±0.05	5.83	0.57±0.06	1.06±0.11	
NCS	5/2-3/2 ef	9/2-7/2	42699.184±0.010	2.25±0.07	5.83	0.67±0.02	3.14±0.10	
	5/2-3/2 ef	7/2-4/2	42702.930±0.010	2.10±0.08	5.83	0.82±0.04	2.39±0.10	
	5/2-3/2 ef	5/2-3/2	43705.851±0.010	1.61±0.08	5.83	0.81±0.05	1.88±0.10	

Notes. ^(a) Main refers to the three hyperfine components with the strongest line intensities, $F_u - F_l = J + 1 \rightarrow J$, $J \rightarrow J - 1$, and $J - 1 \rightarrow J - 2$, respectively. These are unresolved but could produce a measurable line broadening. However, the model to compute the synthetic spectrum of all CHNS isomers and isotopologues takes into account all hyperfine components. ^(b) Observed frequencies for the transitions of the species studied in this work assuming a v_{LSR} of 5.83 km s⁻¹ (see text). For lines for which only upper limits to the intensity are obtained the predicted frequencies from the laboratory data are given. ^(c) Integrated line intensity in mK km s⁻¹. ^(d) Line width at half intensity using a Gaussian fit in the line profile (in km s⁻¹). ^(e) Antenna temperature (in mK). Upper limits correspond to 3σ values. ^(A) These hyperfine components appear too strong compared with the other transition of the same molecule. They are probably blended with unknown lines as shown in Fig. 1. ^(B) Heavily blended line. Derived parameters are uncertain (see Fig. A.2). ^(C) The hyperfine components are blended but produce a well-defined line profile. The line width has been fixed to 0.6 km s⁻¹ (see Fig. A.2). ^(D) The main component is affected by a line of HC₄N at +8 MHz in the frequency switching data with a throw of 8 MHz, and by a line of c-C₃HCCH at -10 MHz in the data with a throw of 10 MHz. The corresponding line parameters are uncertain (see Fig. A.3).

Table A.2. Observed line parameters for the isomers and isotopologues of HNCO

Species	$J_u - J_l$	$F_u - F_l^a$	ν_{rest}^b (MHz)	$\int T_A^* d\nu^c$ (mK km s ⁻¹)	v_{LSR} (km s ⁻¹)	$\Delta\nu^d$ (km s ⁻¹)	$T_A^*^e$ (mK)	Notes
HNCO	$2_{02} - 1_{01}$	1-1	43962.015±0.010	21.16±0.10	5.83	0.63±0.01	31.17±0.14	
		1-2	43962.626±0.010	1.15±0.09	5.83	0.58±0.05	1.86±0.14	
		3-2	43963.013±0.010	174.41±0.01	5.83	0.72±0.01	229.15±0.14	A
		2-1						A
		1-0	43963.556±0.010	29.93±0.12	5.83	0.67±0.05	42.19±0.14	
	$4_{04} - 3_{03}$	2-2	43963.659±0.010	18.87±0.11	5.83	0.59±0.05	29.71±0.14	
		3-3	87924.350±0.010	10.42±1.68	5.83	0.58±0.10	16.89±2.02	
		Main	87925.238±0.010	307.62±1.58	5.83	0.63±0.01	525.21±2.02	
	$5_{05} - 4_{04}$	4-4	87925.921±0.010	8.94±1.53	5.83	0.60±0.11	14.12±2.02	
		Main	109905.734±0.010	175.38±1.31	5.83	0.51±0.01	324.74±3.67	
HN ¹³ CO	$2_{02} - 1_{01}$	3-2	43964.265±0.010	3.41±0.04	5.83	0.74±0.02	4.33±0.14	A
		2-1					A	
		1-0	43964.807±0.010	0.58±0.03	5.83	0.57±0.04	0.94±0.14	
		2-2	43964.897±0.010	0.29±0.04	5.83	0.48±0.15	0.70±0.14	
H ¹⁵ NCO	$2_{02} - 1_{01}$		42646.445±0.010	0.73±0.09	5.83	0.59±0.09	1.15±0.10	
DNCO	$2_{02} - 1_{01}$	1-1	40785.534±0.010	0.54±0.10	5.83	0.58±0.11	0.87±0.07	
		3-2	40786.545±0.015	1.65±0.10	5.83	0.60±0.15	2.12±0.07	B
		2-1	40786.618±0.015	1.28±0.10	5.83	0.60±0.15	1.98±0.07	B
		1-0	40787.139±0.015	0.66±0.08	5.83	0.60±0.15	0.79±0.07	B
		2-2	40787.249±0.015	0.48±0.08	5.83	0.60±0.15	0.69±0.07	B
	$4_{04} - 3_{03}$	Main	81571.895±0.010	6.34±0.37	5.83	0.57±0.02	10.42±0.66	
HCNO	2-1	Main	45876.059±0.010	7.16±0.12	5.83	0.91±0.02	7.41±0.15	C
	4-3	Main	91751.350±0.010	2.11±0.60	5.83	0.30±0.10	6.60±1.68	C,D
DCNO	2-1	Main	41169.798±0.010	0.25±0.05	5.83	0.54±0.10	0.44±0.08	C
HOCN	$2_{02} - 1_{01}$	2-2	41949.966±0.010	1.54±0.09	5.83	0.61±0.05	2.36±0.15	
		1-0	41950.108±0.010	2.14±0.09	5.83	0.64±0.04	3.14±0.15	
		2-1	41950.848±0.010	5.22±0.25	5.83	0.70±0.15	6.79±0.15	B
		3-2	41950.902±0.010	6.97±0.25	5.83	0.70±0.15	9.99±0.15	B
		1-1	41952.292±0.010	1.78±0.20	5.83	0.69±0.06	2.45±0.15	
	$4_{04} - 3_{03}$	Main	83900.560±0.010	12.77±0.53	5.83	0.62±0.03	19.35±0.61	
	$5_{05} - 4_{04}$	Main	104874.696±0.010	4.44±0.77	5.83	0.32±0.06	13.11±2.53	
	NCO	7/2-5/2e	9/2-7/2	81404.306±0.015	2.08±0.26	5.83	0.67±0.10	2.92±0.53
7/2-5/2f		9/2-7/2	81404.815±0.015	1.40±0.23	5.83	0.51±0.10	2.55±0.53	
7/2-5/2e		7/2-5/2	81413.143±0.020	0.81±0.25	5.83	0.47±0.14	1.62±0.65	
7/2-5/2f		7/2-5/2	81413.591±0.020	0.66±0.21	5.83	0.32±0.14	1.93±0.65	

Notes. ^(a) Main refers to the three hyperfine components with the strongest line intensities, $F_u - F_l = J + 1 \rightarrow J$, $J \rightarrow J - 1$, and $J - 1 \rightarrow J - 2$, respectively. These are unresolved but could produce a measurable line broadening. However, the model to compute the synthetic spectrum of all CHNO isomers and isotopologues takes into account all hyperfine components. ^(b) Predicted, or observed, frequencies for the transitions of the species studied in this work (see text). ^(c) Integrated line intensity in mK km s⁻¹. ^(d) Line width at half intensity using a Gaussian fit in the line profile (in km s⁻¹). ^(e) Antenna temperature (in mK). ^(A) The $F = 3-2$ and $F = 2-1$ hyperfine components are blended with a predicted separation between them of 40 kHz. The derived frequency corresponds to that of the averaged value of both components. ^(B) The hyperfine components are blended. The line width has been fixed. We estimate an uncertainty on this parameter of 0.15 km s⁻¹. ^(C) The hyperfine components are blended. A single line has been fitted (see Fig. A.4). ^(D) Blended with a U-line as shown in Fig. A.2 but line parameters can be still estimated.